

Master Thesis

Towards lifelong mapping in pointclouds

Panagiotis Chatzichristodoulou

Master Thesis DKE 09-16

Thesis submitted in partial fulfillment
of the requirements for the degree of Master of Science
of Artificial Intelligence at the Department of Knowledge
Engineering of the Maastricht University

Thesis Committee:
University of Maastricht
Rico Mockel, Kurt Driessens
Distributed Organisms B.V.(DoBots)
Anne Van Rossum

Maastricht University
Faculty of Humanities and Sciences
Department of Knowledge Engineering
Master Artificial Intelligence

August 8, 2015

Abstract

Long term mapping is the natural conceptual extension to existing mapping methods that are focused on mapping static environments. Mapping an area for a large amount of time is a problem that if tackled efficiently will be a large step towards fully autonomous robots. As discussed in the literature lifelong mapping consists of two major subproblems. A compression, and a dynamic environment problem. This thesis discusses the application of non parametric Bayesian methods and how such tools can be directed to tackle the clustering subproblem of lifelong mapping methods. A novel method of pointcloud representation is presented and its results are applied to an EKF SLAM algorithm; its strengths and weaknesses are analyzed as well as the directions in which the method could be extended to be a complete solution to both the dynamic as well as the compression problem of lifelong mapping.

CONTENTS

1	Introduction	4
2	Literature review	5
2.1	Object based SLAM	5
2.2	Point Cloud Object clustering	6
2.3	Non Parametric Bayesian methods	6
2.4	Correspondence	6
3	Theory background	7
3.1	Dirichlet Distribution	7
3.2	Sampling methods	8
3.2.1	Stick Breaking Process	8
3.2.2	Polya's Urn	9
3.3	Dirichlet Process	10
3.4	Sampling methods	10
3.4.1	Chinese restaurant process	10
3.4.2	Stick Breaking	11
3.5	Dirichlet process mixture models	11
3.6	Inference	13
3.7	Generalized Polya Urn	13
4	Model definition	14
4.1	General pipeline	15
4.2	The data distribution	16
4.3	Sequential monte carlo sampler	18
4.3.1	Gibbs updates	19
4.3.2	Weight updates	20
4.4	Decision Layer	20
4.5	Complexity	20
4.6	Landmark size	22

5 Results	22
5.1 Simple datasets	22
5.2 Expressiveness and decision layer	24
5.3 EKF-SLAM experiments	26
5.3.1 Speed	27
5.3.2 Memory requirements	28
5.4 Discussion	29
5.4.1 Unsupervised learning	29
5.4.2 Clustering layer	29
5.4.3 Decision layer	30
6 Conclusion and future work	31

LIST OF FIGURES

1 Different behaviour the distribution for different initial parameters of the α vector	8
2 Stick breaking construction	9
3 Poly's urn for $\alpha=[2 \ 1 \ 1]$	9
4 The CRP process	11
5 The stick breaking process for Gaussian base distribution and different values of alpha	12
6 Mixture model	12
7 A Dirichlet process mixture model.	13
8 GPU as a function of CRP	14
9 General landmark update pipeline	15
10 Point cloud modification pipeline.	16
11 Exponential trend	16
12 Initial data along with the distributions inferred	23
13 More complicated color distributions	25
14 The colour and position boudnary is displayed in these pictures	26
15 SLAM session using the pipeline.	27
16 Memory Requirements as a function of strength parameter α	29
17 Fail use cases.	30
18 Fail use cases.	31

1. INTRODUCTION

Simultaneous Localization And Mapping(slam) is one of the fundamental problems of autonomous systems[1]. In order for robots to be considered truly autonomous they have to be able to enter an environment and map its structure. In that direction we can now efficiently map such environments with solutions like EKF-slam[2] and FastSlam[40]. The logical extension of methods that can map static environments is methods that remove this restriction. The idea of lifelong learning in robots is not new[5], and in recent years research with a specific focus on lifelong learning in mapping[6] was introduced. Lifelong mapping introduces the concept of robots that are able to continuously map their environment and this leads to two basic extensions over existing methods: Mapping methods must be able to handle the memory needs of an environment that constantly increases and mapping methods must be robust enough to be able to handle dynamic environments and the changes they introduce to the map over time.

As a result, lifelong mapping consists of two basic subproblems: a compression problem as the map increases over time and a dynamic environment problem as the environment changes over time[7]. In this project the focus will be directed on the compression problem of lifelong mapping. More specifically, how can Bayesian non-parametric methods be used to create compressed environment representations that still retain enough information to be used as reference points when performing slam. The following research questions have then to be addressed: Are such representations rich enough to be used as references points when performing slam? Are the clustering methods fast enough to be used in online methods? Is the compression created by the methods significant? Since different sensors require different approaches the focus will be directed on methods that use RGBD sensors like Microsoft Kinect to perform the mapping.

Since its introduction in 2010 Microsoft Kinect[25] has revolutionized rgbd devices with its low price range and high quality sensors. It came as no surprise that research in pointclouds, the cloud representation system of Kinect, has increased since then. Many libraries that enable the user to perform tasks from feature extraction to plane segmentation[12] in pointclouds are currently available. In the field of robotics, many teams are using the Kinect sensors to perform simultaneous localization and mapping[13]. The goal of this thesis is to introduce a novel approach to tackle the compression problem of lifelong mapping methods that use the Kinect devices while using Bayesian non parametric methods as the base of its solution.

Dirichlet processes and Dirichlet process mixture models [26] are the cornerstone of Bayesian non-parametric statistics. The strength of those models lies in the fact that they allow the model's mixture components to grow as much as needed so as to best fit the data. The dynamic number of components in combination with different prior choices leads to very flexible models that can be used in a very large area of applications from topic modeling[43] to speaker diarization[45]. The main motivation of this project is to use such methods as a means of creating compressed representations of the environment that also retain enough expressiveness to be used as reference points when performing slam. In this paper a novel compressed representation of a cloud is introduced and its results are analyzed both towards their robustness and expressive ability. The strengths and weaknesses of the method are analyzed and directions on how the method could be extended to tackle all the rest subproblems of Walcott's thesis is given in the discussion section.

The rest of the paper is structured as follows. Section 2 will present relevant literature review, Section 3 will introduce the theories behind the model, Section 4 will define the model, Section 5

will show experimental results of the method. Finally, Section 6 will end up with a conclusion and future directions in which the method could be improved.

2. LITERATURE REVIEW

Literature review will be focused on 4 related sub fields: Object based SLAM, pointcloud object segmentation, non-parametric bayesian methods and the correspondence problem in SLAM.

Given that the idea behind the project is to create representations of objects within the cloud, methods that use objects to perform SLAM are relevant. The second part of the literature research is focused on point cloud segmentation and the features needed to be extracted from a cloud to optimally segment it to its components. The third part of the research is focused on non-parametric Bayesian methods and the clustering tools they provide. Finally, literature review is focused on the correspondence problem in SLAM. As one of the fundamental problems that need to be solved in order to have robust SLAM algorithms, it is imperative the correspondence problem be solved efficiently.

2.1. Object based SLAM

Object based slam introduces a specific category of slam problems where objects are used as reference points while navigating through the environment. Salas-Moreno et al.[14] define a method of performing object based slam for specific classes objects. The objects are identified by a camera that is on top of the robot. By having a model of pre-trained objects, SLAM can be performed on environments the robot knows what objects to expect. Castle et al. use object recognition to perform object based SLAM with the use of a hand-held cameras. Selvatici et al.[15] use a similar approach while exploiting structural information such as object height and position within the room. That way a couch that is a large object situated in floor level is easier to be recognized. Choudhary et al.[17] use pointclouds and an object database to match objects currently seen with known objects within their database. They use omnimap[27] as their mapping method and as a representation a combination of the downsampled voxel grids with additional normal and curvature information. Finally, all their operations are done in the non-planar components of the pointcloud. Jensfelt et al[15] present an object based approach to SLAM where the robot can manipulate the objects of the map. They use camera pictures as input and receptive Field Histogram as the method to abstract the camera input and extract features for their object matching algorithm. Their approach is proposed as a solution to a service robot scenario. MonoSLAM[19] introduces a method of performing slam using a monocular camera. Seongyong Koo et al.[20] introduce a method of unsupervised object individuation from RGB-D image sequences. They cluster their initial cloud into candidate objects using Euclidian clustering and proceed to extract features like the Euclidian distance(L2) and the Kullback-Leibler distance between pointcloud objects. They use IMFT to solve their tracking problem.

The common base of all the methods in object based slam is that they treat the problem of object based slam as a classification task. More specifically, the robot cannot navigate in environments where it cannot find such objects. The approach presented in this paper introduces a general and unsupervised method of using environment signatures as reference points to perform slam.

2.2. Point Cloud Object clustering

Point cloud clustering tools enable the user to cluster the points of a cloud. The robustness of the clustering varies with respect to the method used the features it requires as well as the application domain. Trevor et al.[29] take positional information, Euclidean distances and the normal of points to as input to their function and output segments that are part of the same object. PCL library[12] introduces methods like Euclidean clustering and conditional Euclidean clustering that use a number of heuristics that take normal as well as curvature information to extract segments in the pointcloud that represent objects. Furthermore, there is a lot of research on segmentation of pointclouds in scenes, with the emphasis usually put on extracting geometric primitives[30],[31] using cues like normals and curvature. Rabbani et al.[23] introduce a new method of object segmentation using KNN as their base algorithm. They also present a very informative literature review along with the strengths and weaknesses of existing methods. Finally Triebel et al.[32] introduce a general clustering framework that does not rely on plane segmentation. Instead of segmenting the plane by using classical approaches like RANSAC or MLASAC they introduce a framework where they make no assumptions regarding plane data. In this paper an alternative novel clustering approach will be introduced that will use Bayesian non-parametric methods as its basis.

2.3. Non Parametric Bayesian methods

Dirichlet processes and Dirichlet process mixture models are the cornerstone of Bayesian statistics. In this project the focus is directed towards the clustering methods that are being introduced by those tools. Radford M. Neal[38] with his paper regarding MCMC methods for Dirichlet process mixture models made the definitive step towards Dirichlet process mixture models(DPMM's) receiving a lot of attention. Since then, a variety of approaches for inference on such models has been introduced with MCMC methods, and variational inference(VI) methods being two prominent such approaches. Variational inference for DPMM's, introduced by Jordan et al.[39] introduces deterministic tools to perform inference and approximate the posterior distribution and marginals of a dataset. Both methods have strengths and weaknesses and many tools have been established by using the two approaches as their base. Blei et al. [43] introduced LDA as a method to perform topic modelling. Teh et al.[41] introduce a hierarchy on the inference process by introducing the Hierarchical Dirichlet process. Particle filter approaches have also been established. Doucet et al.[42] introduce Sequential Monte Carlo as a fast way to approximate inference. Dirichlet process mixture models are a very active research field and covering it is beyond the scope of this thesis. In this project SMC samplers were used due to their robustness as well as their inherent extensiveness. A detailed description on the mechanisms of sequential samplers will be given in the theory section.

2.4. Correspondence

In its general definition, the correspondence problem refers to the problem of ascertaining which parts of one image correspond to which parts of another image, where differences are due to movement of the camera, the elapse of time, and/or movement of objects in the photos. Under the object based SLAM context, it refers to the problem of identifying objects as ones that have been

encountered before during the mapping process. In that direction, Cree et al.[34] create a histogram of line segments of each landmark and compute their root mean square error. They then proceed to calculate their RGB signature to calculate the distance between different landmarks. Low et al.[35] match Scale Invariant Feature Transform (SIFT) features, an approach which transforms image data into scale-invariant coordinates relative to local features. Lamon et al.[36] store a database of fingerprints which indicate the location in the robot's environment. The features are ordered and stored at a database as they appear in the robot's immediate surroundings. A new fingerprint is computed for each new view and matched against existing ones. Finally, in Seghal et al.[37] an extension of SIFT descriptors to 3D data and pointclouds is given. In this paper the correspondence problem is solved using a simple decision layer that compares current environment representations to past ones.

3. THEORY BACKGROUND

An introduction to the Dirichlet Distribution and Dirichlet process mixture models will be given. Finally, the Generaly Polya urn model will be presented as it serves as the base to the sampler presented in the model section.

3.1. Dirichlet Distribution

An example of a *probability mass function*(pmf) is an ordinary six-sided dice. To sample from the pmf, you cast the dice and get a number from 1 to 6. One important property of pmfs given from real dice is that they are not uniformly weighted due to the manufacturing process not being perfect. A bag of dice can then be considered as an example of a random pmf. To sample from this random pmf, you have to put your hand in the bag and draw a die, and the result of this drawing process is itself a probability distribution. A Dirichlet distribution is an object that can be used to model the randomness of such objects whose domain is itself a probability distribution i.e it is a distribution of distributions.

Formally, a probability mass function with k components lies on the $(k-1)$ dimensional probability simplex, which is a surface in \mathbb{R}^k denoted by Δ_k and defined to be the set of vectors whose k components are non-negative and sum up to 1, that is: $\Delta_k = \{q \in \mathbb{R}^k \mid \sum_{i=1}^k q_i = 1, q_i \geq 0 \text{ for } i = 1, 2, \dots, k\}$. Δ_k is itself a $(k-1)$ dimensional object lying in the k dimensional space.

Dirichlet distribution: Let $Q = [Q_1, Q_2, \dots, Q_k]$ be a random pmf, that is, $Q_i \geq 0$ for $i = 1, 2, \dots, k$ and $\sum_{i=1}^k Q_i = 1$. In addition, suppose that $\alpha = [\alpha_1, \alpha_2, \dots, \alpha_k]$, with $\alpha_i \geq 0$ for each i , and let $\alpha_0 = \sum_{i=1}^k \alpha_i$. Then Q is said to have a Dirichlet distribution with parameter α , which we denote by $Q \sim Dir(\alpha)$, if it has $f(q; \alpha) = 0$ if q is not a pmf, and if q is a pmf then:

$$f(q; \alpha) = \frac{\Gamma(\alpha_0)}{\prod_{i=1}^k \Gamma(\alpha_i)} \prod_{i=1}^k q_i^{\alpha_i - 1}$$

The first two cumulants of the distribution are the following:

$$E[\alpha_i] = \frac{\alpha_i}{\alpha_0}$$

$$Cov(Q_i, Q_j) = \begin{cases} \frac{-\alpha_i \alpha_j}{\alpha_0^2 (\alpha_0 + 1)} & \text{if } i \neq j \\ \frac{-\alpha_i (\alpha_0 - \alpha_i)}{\alpha_0^2 (\alpha_0 + 1)} & \text{if } i = j \end{cases}$$

The mean and variance formulas help understand how the changing the α vector affects the behaviour of the distribution as to where the density is located as well as the variance in the pmfs sampled. The following graphs display the difference of behaviour on samples from Dirichlet distributions with different initial alpha values.

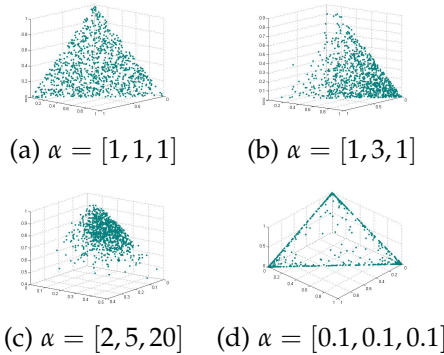


Figure 1: Different behaviour the distribution for different initial parameters of the α vector

Random samples from a Dirichlet distribution are presented in Fig.1. It must be noted that every point within the simplex can be considered itself a pmf since its components add up to one. Furthermore, for an $\alpha = [c, c, c], c \geq 0$, the density is symmetric towards the center of the simplex; for the special case of $\alpha = [1, 1, 1]$ where $c=1$ is displayed at Fig.1(a) where the initial choice of the α vector results in a uniform distribution of points over the probability simplex. As c increases the distribution is concentrated towards the center of the simplex. The behaviour of the density changes when the α vector is not symmetric, when there is a shift in density towards the higher parameter, as is shown in Fig.1(b) and Fig.1(c). Finally, when the values of the vector are smaller than 1, the density of the distribution is shifted towards the vertices of the simplex as is shown in subplot Fig.1(d).

One important property of the Dirichlet distribution is that it serves as a conjugate prior for the probability parameter q of the multinomial distribution. That is, if $(X|q) \sim \text{Multinomial}_k(n, q)$ and $Q \sim \text{Dir}(\alpha)$ then $(Q|X = x) \sim \text{Dir}(\alpha + x)$

3.2. Sampling methods

Two basic sampling methods from the Dirichlet Distribution will be presented: Stick breaking process, and Polya's urn.

3.2.1 Stick Breaking Process

The stick breaking process can be thought of as follows: Imagine breaking a unit length stick into k such that the k pieces follow a $\text{Dir}(\alpha)$ distribution. Such samples can be created by the following procedure:

- **Step 1:** Simulate $u_1 \sim \text{Beta}(a_1, \sum_{i=1}^k a_i)$, and set $q_1 = u_1$. That's the first piece of the stick, with the remaining piece having length of $1 - u_1$
- **Step 2:** For $2 \leq j \leq k - 1$, if $j-1$ pieces, with lengths $u_1, u_2, \dots, u_{j-1}, \dots$ have been broken off, the length of the remaining stick is $\prod_{i=1}^{j-1} (1 - u_i)$. We simulate $u_j \sim \text{Beta}(a_j, \sum_{i=j+1}^k a_i)$ and set $q_j = u_j \prod_{i=1}^{j-1} (1 - u_i)$. The length of the remaining part of the stick is $\prod_{i=1}^j (1 - u_i)$
- **Step 3:** The length of the remaining piece is q_k .

Since the last part of the stick will always be created so that we end up with a valid pmf, it is made explicit how the density of the Dirichlet is a $k - 1$ dimensional object lying in the k dimensional space. Fig.2 shows realizations of the stick breaking process in R^3 and the similarities between the stick breaking sampling method and the probability simplex presented in the previous section are shown.

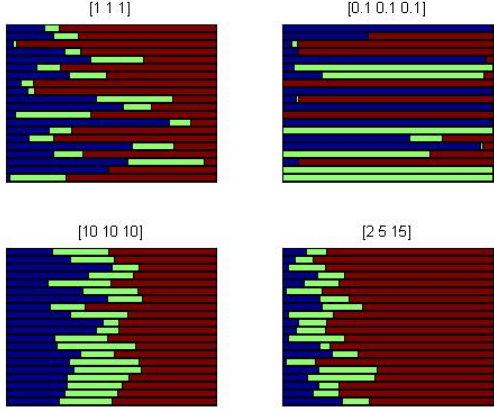


Figure 2: Stick breaking construction

As expected, an initial α vector of $[1,1,1]$ results in a uniform distribution of weights and. Furthermore, as the weights increase we have a more balanced distribution of weights as shown for the case of Fig.2([10,10,10]) and this this balance is shifted towards the higher weight when the initial vector is not symmetric as shown in Fig.2([2,5,15]). Finally, an initial vector of weights < 1 results in single values dominating the simplex.

3.2.2 Polya's Urn

The second method of sampling from a Dirichlet distribution is by using an urn model. In probability theory and statistics, an urn problem is an idealized mental exercise in which some objects of real interest are represented as colored balls in an urn or other container. More specifically, Polya's urn model depicts a random process whose realizations are realizations of a Dirichlet distribution. Suppose that you want to generate $Q \sim Dir(\alpha)$. To start, we put α_i balls of colour i for $i = 1, 2, \dots, k$ in an urn, as shown in Fig.3. It must be noted that α can be fractional and even irrational(!). At each iteration we randomly draw a ball from the urn and put it back in the urn with an extra ball of the same colour as well. As we iterate this procedure an infinite amount of times, the proportions of the balls of each colour will converge to a pmf that is a realization of from the distribution $Dir(\alpha)$.

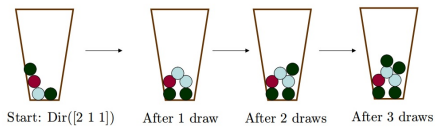


Figure 3: Polya's urn for $\alpha=[2 1 1]$

$Dir(\alpha)$ with an initial vector α .

The procedure can be then described as follows:

- **Step 1:** Set a counter $n=1$. Draw $X \sim \alpha / \alpha_0$.
- **Step 2:** Update counter to $n+1$. Draw $X_{n+1} | X_1, X_2, \dots, X_n \sim \alpha / \alpha_{n0}$, where $\alpha_n = \alpha + \sum_{i=1}^n \delta_{X_i}$ and α_{n0} is the sum of the entries of α_n . Repeat step 2 an infinite number of times.

As the number of iterations of Step 2 approaches infinity, the proportions of ball colors in the simplex will be a realization from the distribution

3.3. Dirichlet Process

The Dirichlet process was formally introduced by Thomas Ferguson in 1973 and serves as an extension to the Dirichlet distribution in modelling infinite sets of events. More specifically, in the introductory example, a six sided dice was described. If instead of a six sided dice a dice with an infinite amount of sides was used, the Dirichlet Distribution could not handle the infinite sample space. A Dirichlet process is a random process whose realizations are distributions over an arbitrary and possibly infinite sample space. To make the infinity assumption manageable, the Dirichlet process restricts the class of distributions it can handle to a specific set: Discrete distributions over the infinite sample space that can be written as an infinite sum of indicator functions which can be formally presented as:

$$P(B) = \sum_{k=1}^{\infty} p_k \delta_{y_k}$$

Where p_k is the mixture weight and δ_{y_k} is an indicator function such that $\delta_{y_k}(B) = 1$ if $y_k \in B$ and $\delta_{y_k}(B) = 0$ otherwise. This formulation makes explicit the fact that realizations of a Dirichlet process are discrete distributions.

Formally, the DP is defined as follows: Let \mathcal{X} be a set and let \mathcal{B} be an σ -algebra on \mathcal{X} . Let $(\mathcal{X}, \mathcal{B})$ denote the collection of probability distributions on set as \mathcal{P} . \mathcal{P} is a Dirichlet Process as with a strength parameter α and a base distribution H on $(\mathcal{X}, \mathcal{B})$ if for any finite measurable partition $\{B_i\}_{i=1}^k$ of \mathcal{X} , the random vector $((P(B_1), \dots, P(B_k))$ has a Dirichlet distribution with parameters $(\alpha H(B_1), \dots, \alpha H(B_k))$. The mean and the covariance of a Dirichlet process are defined as:

- $\mathcal{E}[G(A)] = \alpha H(A)$. The base distribution can be thought of as the mean of the Dirichlet process
- $\mathcal{V}[G(A)] = \frac{H(A)(1-H(A))}{\alpha+1}$. The strength parameter α can be thought of as the inverse covariance of the Dirichlet process.

3.4. Sampling methods

Two methods for sampling from a Dirichlet process will be presented: the Chinese Restaurant Process, the Stick Breaking Process.

3.4.1 Chinese restaurant process

Polya's Urn and the stick breaking process are two names of the same process. The Chinese restaurant process paradigm is similar to the Polya's urn and it is defined as follows: Imagine a restaurant with an infinite number of tables, each with infinite capacity. At time $t=1$, the first customer enters the restaurant and sits at table 1 with probability 1. For every next step, the customer can either

- Choose an unoccupied table with probability $\propto \frac{\alpha}{n-1+\alpha}$
- Choose occupied table k with probability $\propto \frac{c}{n-1+\alpha}$ where c is the number of people currently sitting at that table

If you let an infinite number of customers enter the restaurant, the proportions of people sitting on each table will be a realization from a Dirichlet process with strength parameter α .

It can be seen that there is a positive reinforcement effect in this process, that is the more people already sitting at a table, the bigger the probability that more people will be sitting into that table in the future. It can also be proved that the number of tables grows $\propto \alpha \log(n)$ where n is the number of customers in the restaurant. Fig.4 visualizes the progression of the process as more people enter the restaurant.

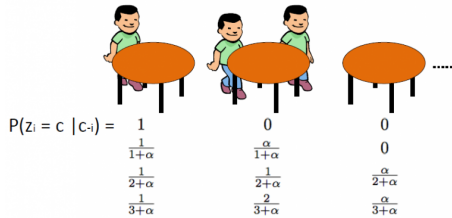


Figure 4: The CRP process

One important property of this procedure is that the n th customer has the same probability to sit on the same table as any other customer of the table. That is the number of people seating on table 1 is on average the same as the number of people seating on table k ! This very interesting and counter intuitive(at first) property of the exchangeable data and understanding this is crucial on building intuition regarding the behaviour of exchangeable random variables.

3.4.2 Stick Breaking

Measures drawn from a Dirichlet distribution are discrete with probability 1. This property is made explicit by the stick breaking construction. The construction is based on the independent sequences of i.i.d. random variables $(\pi'_k)_{k=1}^{\infty}$ and $(\phi_k)_{k=1}^{\infty}$ defined as follows:

$$\pi'_k | \alpha_0, G_0 \sim Beta(1, \alpha_0) \quad \phi_k | \alpha_0, G_0 \sim G_0$$

This can be defined as follows: Draw π'_k as a Beta random variable. Draw ϕ_k from G_0 . Now define a random measure G as:

$$\pi_k | \pi'_k \prod_{l=1}^{k-1} (1 - \pi'_l) \quad G = \sum_{k=1}^{\infty} \pi_k \delta_{\phi_k}$$

The first part of the stick will have length π'_k and the conditional length given all the previous draws is given by π_k . Finally, the distribution created is given as an infinite sum of indicator functions given by G . Fig.5 displays a Dirichlet Process's realization from a stick breaking process with a Gaussian base distribution. Different parameter values for strength parameter α directly affect the distributions output. As the alpha parameter is increased, the realization of the distribution will be closer to the base distribution. Furthermore, this picture also shows that the distribution created from the infinite sum of indicator function is a discrete distribution. Finally, when G is generated using a stick breaking process with a strength parameter α , it can be written in shorthand as: $G \sim GEM(\alpha)$

3.5. Dirichlet process mixture models

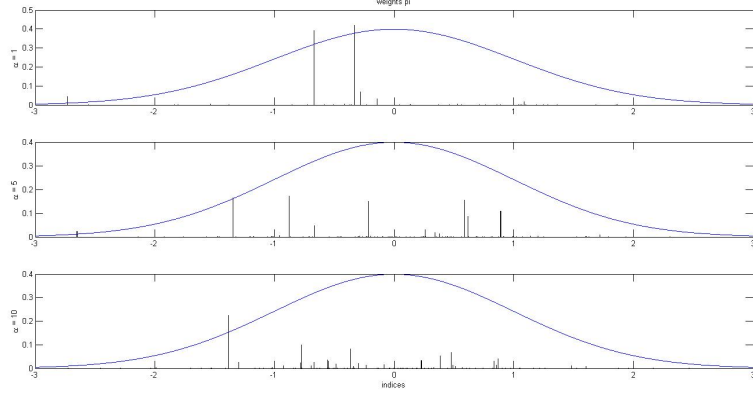


Figure 5: The stick breaking process for Gaussian base distribution and different values of alpha

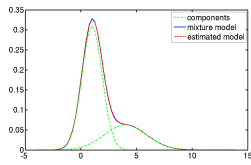


Figure 6: Mixture model

One of the most important properties of those objects is that they can serve as a non-parametric prior to mixture models. A typical 1D mixture model that represents data coming from a mixture of two one-dimensional Gaussian distributions is shown in Fig.6.

Mixture models can be considered as the Bayesian approach to clustering, and one of the most important applications of the Dirichlet process is to serve as the non-parametric prior on the parameters of such models. In particular, suppose that observations x_i arise from the following model:

$$\theta_i | G \sim G, x_i | \theta_i \sim F(\theta_i) \quad (1)$$

Where $F(\theta_i)$ denotes the distribution of the observation x_i given θ_i . The factors θ_i are conditionally independent given G , and the observation x_i is conditionally independent of the other observations given the factor θ_i . When G is distributed according to a Dirichlet process, this model is referred as a Dirichlet process mixture model and its representation is shown in Fig.7. The number of distributions that underlie the data can be mapped to the number of tables within a Chinese restaurant process, and the mixing proportions are proportional to the number of people sitting in every table.

Since G can be represented using a stick-breaking construction, the factors θ_i take on values ϕ_k with probability π_k . We can denote this using z_i as an indicator variable which takes on positive values and is distributed according to π . Hence, an equivalent representation of a Dirichlet process mixture model is given by the following conditional distributions:

$$\begin{aligned} \pi | \alpha_0 &\sim GEM(\alpha_0) & z_i | \pi &\sim \pi \\ \phi_k | G_0 &\sim G_0 & x_i | z_i, (\phi)_k^{\infty} &\sim F(\phi_{z_i}) \end{aligned} \quad (2)$$

The infinite limit of finite mixture models is taken when we let the number of components into a model to reach infinity. An infinite mixture model assumes that the data come from an infinite number of distributions.

This means that in such models the number of components from which the data are generated can be infinite. In such models it is important to notice in a dataset of size n , the data come from at most n components. This is an important property of infinite mixture models and is exploited when performing posterior inference.

3.6. Inference

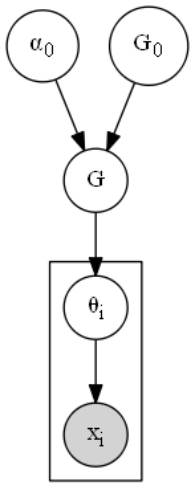


Figure 7: A Dirichlet process mixture model.

Statistical inference is the process of deducing properties of an underlying distribution by analysis of data. Inference can be considered as the inverse procedure presented in the plate in Fig.7; the same graphical process with the arrows facing the opposite direction. Statistical inference techniques can be categorized into 3 families: MCMC, Variational inference and SMC methods. The literature on such methods is extensive and covering it is beyond the scope of this project; for the purpose of this project an SMC sampler will be defined in detail in the model definition section.

3.7. Generalized Polya Urn

Dirichlet process priors have been widely used in the literature as non-parametric Bayesian tools to estimate the number of clusters in the data[46]. Dependent Dirichlet Processes(DDP) extend those tools by allowing the clusters in the data to vary with some variance over time by introducing dependencies on the data. The DDPs are a natural extension of the Dirichlet processes in domains where data cannot be considered exchangeable.

A DDP is also known as Generalized Polya Urn[47]. The most important property of this model is that it randomly deletes partitions of clusters on every iteration.

This Generalized Polya Urn distribution also has the shorthand notation GPU(α, ρ) and can be described as follows: At time point t given the clusters at $t - 1$ and the data N_{t-1} perform the following: for every cluster and every point within that cluster the point will stay in the cluster or be deleted from it; the probability of a point being deleted from the cluster is proportional to either the size of the cluster or a constant value $\rho < 1$ [47]. After the deletion takes place, each point at time t is being assigned to a new cluster $c_{t,n}$ with probability proportional to the size of the cluster at time $t - 1$ or assigned to a new cluster with probability proportional to strength parameter α of the prior Dirichlet Process. Cluster sizes are then updated accordingly.

The GPU can be described using the Chinese restaurant process paradigm as follows: At time t , customers are seating at several tables in the restaurant. Each customer decides if he/she will remain at table with probability p or definitely leave the table with probability $1 - p$. Each customer makes his/her decision and leaves or remains seated. Each table occupied is moved

according to the number of customers still occupying the table or is deleted if is currently empty. A new customer then enters the restaurant and either chooses to sit on one of the existing tables with probability proportional to the numer of customers sitting at that specific table or choose table a new with probability to the strength parameter α of the prior Dirichlet process.

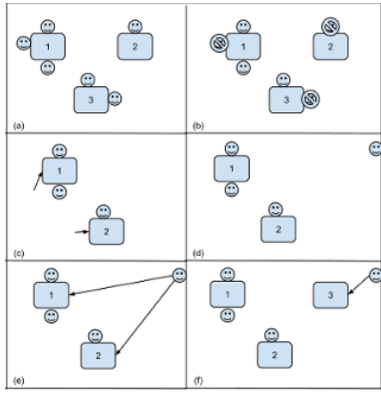


Figure 8: GPU as a function of CRP

Algorithm 1 describes the following process: At time step t given cluster assignments at time $t - 1$ and data N_{t-1} perform the following: for every cluster and every point within that cluster the point will either stay in the cluster or be deleted from it; the probability of a point being deleted from the cluster is proportional to either the size of the cluster or a constant value $\rho < 1$ [47]. Cluster sizes are then modified with respect to the number of points that were deleted from each cluster. After the deletion takes place, each point at time t is being assigned to a new cluster $c_{t,n}$ with probability proportional to the size of the cluster at time $t - 1$ after the deletion step or be assigned to a new cluster with probability proportional to strength parameter α of the prior dependent Dirichlet process. Cluster sizes are then updated accordingly.

Algorithm 1 GPU

```

1: procedure GPU( $t$ )
2:   for  $k = 1, \dots, K_{t-1, N_{t-1}}$  do
3:     Draw  $\Delta s_{t-1}^k \sim \text{Binom}(s_{t-1, N_{t-1}}^k, \rho)$                                  $\triangleright$  Number of elements to delete
4:     Set  $s_{t,0}^k = s_{t-1, N_{t-1}}^k - \Delta s_{t-1}^k$ 
5:   end for
6:   for  $n = 1, \dots, N_t$  do
7:     Draw  $c_{t,n} \sim \text{Cat}\left(\frac{s_{t,n-1}^1}{\alpha + \sum_k s_{t,n-1}^k}, \frac{s_{t,n-1}^2}{\alpha + \sum_k s_{t,n-1}^k}, \dots, \frac{\alpha}{\alpha + \sum_k s_{t,n-1}^k}\right)$ 
8:     If  $c_{t,n} \leq K_{t,n-1}$  set :  $s_{t,n}^{c_{t,n}} = s_{t,n-1}^{c_{t,n}} + 1, K_{t,n} = K_{t,n-1}$ 
9:     If  $c_{t,n} > K_{t,n-1}$  set :  $s_{t,n}^{c_{t,n}} = 1, K_{t,n} = K_{t,n-1} + 1$ 
10:   end for
11: end procedure

```

4. MODEL DEFINITION

The model definition section is structured as follows: An introduction to the general pipeline that will serve as the compressed sensor model of the EKF slam module is presented first. Every non-trivial component of the pipeline is then analysed in detail with respect to the operations it serves.

4.1. General pipeline

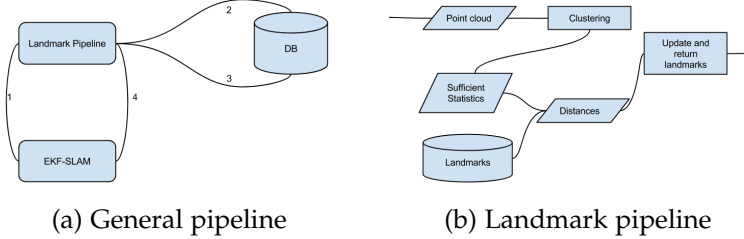


Figure 9: General landmark update pipeline

clusters and returns the landmarks currently being observed while taking into account landmarks that were observed in the past. Landmarks and clusters are identical concepts representing a different layer in the pipeline. More specifically, clusters are output from the sampler and are given as an input of landmarks to the EKF module. Fig. 9 shows a more detailed view of the computations of the pipeline. The algorithmic procedure shown in Algorithm 2 analytically.

Algorithm 2 Landmark Layer

```

1: procedure GETLANDMARKIDs(pointCloud, existingLandmarks)
2:   cloudReduced  $\leftarrow$  downsample(pointCloud)
3:   features  $\leftarrow$  extractFeatures(cloudReduced)
4:   landmarks  $\leftarrow$  cluster(features)
5:   for landmarks as landmark do
6:     (similarity, landId)  $\leftarrow$  calcBestSim(landmark, existingLandmarks)
7:     if similarity  $>$  threshold then
8:       addLandmarks(landMarkIds, landId)
9:     else
10:      newID  $\leftarrow$  addLandmark(landmark)
11:      addLandmarks(newID)
12:    end if
13:   end for
14:   return landMarkIds                                 $\triangleright$  Return landmarks
15: end procedure

```

Method input: The method takes as input a pointcloud as it is currently being read by the kinect sensor.

Lines 3-4: The downsampling and feature extraction are done through the pcl[12] library. A voxel grid is used to reduce the dataset size. A leaf size of approximately 3cm produces a good trade-off between precision and speed. The object representation used approach is similar to[17]. Instead of using the CSHOT descriptor, fpfh[22] histogram is used instead. A fast point feature

histogram(fpfh) represents an angular signature between a point and its neighbors. After the fpfh estimation an angular signature of information between a point and its neighbors is acquired. The color signature of the cloud is being encoded with an approach similar to [33]. The color spectrum is discretized and what is extracted is the count of different color signatures between a point and its k nearest neighbors. Finally the position of every point is also given as input to the algorithm. The pipeline is presented in figure Fig. 10. The pipeline outputs a vector of $\mathbf{x} = (x_s, x_c, x_a)$ where s represents a vector of space information, c a vector of colour information and a angular information.

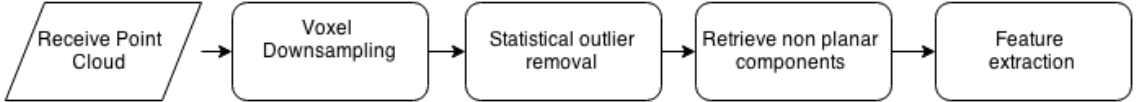


Figure 10: Point cloud modification pipeline.

Lines 5: The input of the method is the feature vector for every data point which is calculated in the previous steps. The clustering is done using the SMC sampler presented in section 4.3.

Lines 6-12: The correspondence of previously seen landmarks to current observations is computed here. Since the landmarks are distributions, statistical distances can be taken to perform the matching. For every observation, its distances with all the stored landmarks are calculated. calcBestSim returns the cluster with the highest similarity that exists in the database. If the similarity is high enough, correspondence is performed and the landmark is added to the landmark list to be send for update in the EKF, otherwise a new landmark is added and its ID is then added to the list.

Lines 15: The algorithm returns the list of the landmarks the robot currently encounters.

4.2. The data distribution

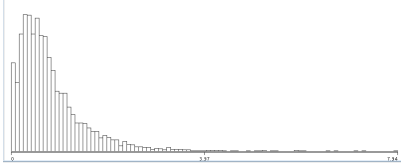


Figure 11: Exponential trend

Each point x in the cloud is represented as a tuple $\mathbf{x} = (x^s, x^a, x^c)$ where superscript s represents spatial information, a angle information, and c color information. The method those features are extracted is explained in lines 3 and 4 of the general pipeline.

The object model is a mixture of distributions over the data with each object being modeled as $F(\theta_t^k)$ where θ represents the parameters of object k at time t . More specifically, each set \mathbf{X} with n datapoints at time t is distributed as:

$$\mathbf{X}_{t,n} \sim F(\theta_t^k) = \text{Normal}(x_{t,n}^s | \mu_t, \Sigma_t) \text{Mult}(x_{t,n}^c | \delta_t) \text{Exp}(x_{t,n}^a | \lambda_t)$$

Where *Normal* is a three dimensional normal distribution with mean μ and covariance Σ representing the positional distribution of the data; *Mult* is a Categorical multinomial distribution with parameter vector δ representing the color distribution and *Exp* is an exponential with rate λ representing the angle distribution of the data within the cluster. This signature introduces a novel

environment abstraction and the purpose of choosing such signature was to have both simple but also informative environment signatures captured by the model. The exponential distribution specifically was chosen to model angular information after empiric evaluation showed that it would provide a good fit for the angle signature distribution of the data. A typical angle signature distribution is shown in Fig. 11 and the exponential trend of data distances is trivial to distinguish.

Now that the object distribution is defined, the progression of the sufficient statistics at time t given $t - 1$ given by:

$$\theta_t^k | \theta_{t-1}^k \sim \begin{cases} T(\theta_{t-1}^k) & \text{if } k \leq K_{t-1} \\ G_0 & \text{if } k > K_{t-1}. \end{cases}$$

Where T represents the transition kernel of the data given the previous state in the model. The case $k > K_{t-1}$ represents the creation of a new cluster and G_0 is the base distribution of the DDP. In our case, the conjugate priors of the distributions of the data were chosen to model the base distribution. Therefore, G_0 is defined as:

$$G_0(\theta_t^k) = NiW(\mu_t^k, \Sigma_t^k | \kappa_0, \mu_0, \nu_0, \Lambda_0) Dir(\delta_t^k | q_0) Gam(\lambda_t^k | \alpha_0, \beta_0)$$

Where NiW is a Normal inverse Wishart distribution, Dir denotes a Dirichlet distribution, and Gam the Gamma distribution. $\kappa_0, \mu_0, \nu_0, \Lambda_0, q_0, \alpha_0$ and β_0 are parameters of the model. The generative process for the Dependent Dirichlet mixture model can be written for each timestep t as:

-
1. Draw $c_t \sim GPU(\alpha, \rho)$
 2. $\forall k$ draw: $\theta_t^k | \theta_{t-1}^k \sim \begin{cases} T(\theta_{t-1}^k) & \text{if } k \leq K_{t-1} \\ G_0 & \text{if } k > K_{t-1}. \end{cases}$
 3. \forall point n draw $x_{t,n} \sim F(\theta_t^{c_t,n})$
-

The transition kernel must satisfy[47]:

$$\int G_0(\theta_k) T(\theta_t^k | \theta_{t-1}^k) d\theta_{t-1}^k = G_0(\theta_k)$$

The equation means that the invariant distribution must equal its base distribution. A typical way of meeting this restriction and forcing the sampler to converge to the original target density[49] is to introduce a set of M auxiliary variables \mathbf{z} such that:

$$P(\theta_t^k | \theta_{t-1}^k) = \int P(\theta_t^k | z_t^k) P(z_t^k | \theta_{t-1}^k) dz_t^k$$

The transition kernel of the model can now be sampled by using the following formula: $\theta_t^k \sim T(\theta_{t-1}^k) = T_2(z_t^k) \circ T_1(\theta_{t-1}^k)$ where:

$$\begin{aligned} z_{t,1:M}^k &\sim T_1(\theta_{t-1}^k) \\ &= Normal(\mu_{t-1}, \Sigma_{t-1}) Mult(\delta_{t-1}) Exp(\lambda_{t-1}) \end{aligned} \tag{3}$$

$$\begin{aligned} \mu_t, \Sigma_t, \delta_t, \lambda_t &\sim T_2(z_{t,1:M}^k) \\ &= NiW(\kappa_M, \mu_M, \nu_M, \Lambda_M) Dir(q_M) Gam(\alpha_M, \beta_M) \end{aligned} \quad (4)$$

where $\mu_t, \Sigma_t, \delta_t, \lambda_t$ are posterior parameters given the auxiliary variables z .

4.3. Sequential monte carlo sampler

Sequential Monte Carlo(SMC) samplers for Dirichlet process mixture models were introduced by Doucet et al. [50] and serve as fast alternative to Markov Chain Monte Carlo and Variational Inference methods of performing posterior inference. SMC samplers have known strengths and weaknesses and are a good fit for the problem at hand, as their main theoretical disadvantage, the particle degradation is hard to occur at the minimal time horizon that the sampler is being used. We can now define the SMC sampler that will be used to perform inference on our model as follows:

Algorithm 3 SMC for DDPM

```

1: Input: Points  $\{x_{1,1:N_t}, \dots x_{T,1:N_t}\}$  with extracted features
2: Output: Clusters representing of the data
3: for  $t = 1, \dots, T$  do
4:   for  $l = 1, \dots, L$  do
5:     for  $iter = 1, \dots, S$  do
6:       Sample  $(c_t)^{(l)} \sim Q_1$ 
7:       Sample  $(\theta^k) \sim Q_2$ 
8:     end for
9:     for  $k = 1, \dots, K$  do
10:      Sample  $\Delta s_{t-1}^k \sim Binom((s_{t-1,N_{t-1}}^k)^{(l)}, \rho)$ 
11:      Set  $s_{t,0}^k = s_{t-1,N_{t-1}}^k - \Delta s_{t-1}^k$ 
12:      Sample  $((z_{t+1}^k)^{(l)}) \sim T_1((\theta_t^k))^{(l)}$ 
13:    end for
14:    compute particle weights  $w_t^l$ 
15:  end for
16:  Normalize and resample weights
17: end for

```

The process is straightforward and can be described as follows: For every time step T for every particle L and for every sample S , sample cluster indexes $c_t^{(l)}$ from the proposal distribution Q_1 and sufficient statistics from proposal distribution Q_2 . After clusters assignments and sufficient statistics are sampled for all the samples and particles, perform the deletion step of the DDP and sample auxiliary variables with from the transition kernel of the elements that stayed in the clusters after the deletion steps. Compute the weights and perform the resampling.

4.3.1 Gibbs updates

The proposal distribution Q_1 is the probability of an assignment $c_{t,n}$ given cluster sizes, parameters and concentration α . Formally Q_1 can be written as:

$$Q_1(c_{t,n}|s_{t,n}^k, \theta_t^k, \alpha) \propto \text{Cat}(s_{t,n}^1, \dots, s_{t,n}^K, \alpha) \times \begin{cases} F(x_{t,n}^c|\theta_t^{c_t}) & \text{if } k \leq K_{t-1} \\ \int P(x_{t,n}^c|\theta_t)G_0(\theta)d\theta & \text{if } k > K_{t-1} \end{cases} \quad (5)$$

Where $c_{t,n}$ represents cluster c of point n at time t , s represents cluster sizes. The integral represents the posterior predictive distribution of the cluster times the base distribution with the parameters integrated out. More specifically, the analytic expression of the integral is:

$$\begin{aligned} \int P(x_{t,n}^c|\theta_t)G_0(\theta)d\theta &= \int \text{Normal}(x_{t,n}^s|\mu_t, \Sigma_t) \text{Mult}(x_{t,n}^c|\delta_t) \text{Exp}(x_{t,n}^a|\lambda_t) \times \\ &\quad \text{NiW}(\mu_t, \Sigma_t|\kappa_0, \mu_0, \nu_0, \Lambda_0) \text{Dir}(\delta_t|q_0) \text{Gam}(\lambda_t|\alpha_0, \beta_0) d\theta \\ &= \int \text{Normal}(x_{t,n}^s|\mu_t, \Sigma_t) \times \text{NiW}(\mu_t, \Sigma_t|\kappa_0, \mu_0, \nu_0, \Lambda_0) \\ &\quad \text{Mult}(x_{t,n}^c|\delta_t) \times \text{Dir}(\delta_t|q_0) \\ &\quad \text{Exp}(x_{t,n}^a|\lambda_t) \times \text{Gam}(\lambda_t|\alpha_0, \beta_0) d\theta \\ &= t_{\nu_0-1}(x_{t,n}^s|\mu_0, \frac{\Lambda_0(\kappa_0+1)}{\kappa_0(\nu_0-1)}) \times \prod_{j=1}^V \frac{\Gamma(x_{t,n}^c)}{\Gamma(q_0)} \times \\ &\quad \frac{\Gamma(\sum_{j=1}^V q_0)}{\Gamma(\sum_{j=1}^V x_{t,n}^c)} \times \text{Lomax}(\alpha_0 + s_{t,n}^c, \beta_0 \sum_{j=1}^V x_{t,n}^c) \end{aligned} \quad (6)$$

Where t represents student's t-distribution with ν degrees of freedom, Lomax represents Lomax distribution with shape and scale, α and β respectively and the rest represent a Dirichlet-Multinomial(aka DirMul) distribution. The formulas of the posterior predictive distributions can be found in the literature with [48] being a good example.

The conjugacy of the base and prior distribution allows for an easy sampling formula for proposal distribution Q_2 which is of the form:

$$\begin{aligned} Q_2(\theta_t^k|\theta_{t-1}^k, x_t^k, z_t^k) &\propto F(x_t^k|\theta_k) \times T_2(\theta_t^k|z_t^k) \\ &= \text{NiW}(\mu_t^k, \Sigma_t^k|\kappa_n, \mu_n, \nu_n, \Lambda_n) \text{Dir}(\delta_t^k|q_n) \text{Gam}(\lambda_t^k|\alpha_n, \beta_n) \end{aligned} \quad (7)$$

With:

$$\begin{aligned} \kappa_n &= \kappa_0 + N, \nu_n = \nu_0 + N, \mu_n = \frac{\kappa_0}{\kappa_0 + N}\mu_0 + \frac{N}{\kappa_0 + N}\bar{x}^s \\ \Lambda_n &= \Lambda_0 + s_x^s, q_N = q_0 + \sum_n x_i^c, \alpha_n = \alpha_0 + N, \beta_n = \beta_0 + \sum_n x_i^a \end{aligned} \quad (8)$$

Where \bar{x} defines the sample mean for the elements assigned at cluster c , s_x the sample variance and N denotes the number of observations[52].

4.3.2 Weight updates

Finally, the weight update step is defined as follows: On every time step t the weight of particle l is calculated as:

$$w_t^{(l)} = \frac{P(c_t^{(l)}, \theta_t^{(l)}, x_t | \theta_{t-1})}{P(c_t^{(l)}, \theta_t^{(l)} | \theta_{t-1})} \quad (9)$$

Using Bayes rule, the numerator can be written as:

$$P(x_t, | c_t^{(l)}, \theta_t^{(l)}, \theta_{t-1}) \times P(c_t^{(l)}, \theta_t^{(l)} | \theta_{t-1}) \quad (10)$$

Which can be calculated using equations Q_2 and Q_1 for the first and second part respectively. After the particle weights are normalized particles are drawn with probability proportional to their weights.

4.4. Decision Layer

Once the points of the current iteration are clustered, the clusters are passed as input to the decision layer. The decision layer calculates the similarity of the current clusters to past ones; if the similarity is high enough the clusters are considered to be part of the same landmark. To do that, distance measures between the stored clusters and the ones that are inferred at the current iteration of the algorithm must be defined. Distances between distributions are called divergences and a large amount of literature on divergences exists.

Every cluster consists of a three part distribution as it was defined in section 4.2. To define a distance measure between cluster, individual distances between all the distribution parts will be defined. More specifically let l be the distribution of the cluster and o the distribution of a currently observed cluster. l and o can be decomposed into 3 parts: l_G, l_C, l_E where G,C and E stand for Gaussian, Categorical and Exponential respectively. With that notation the distances between those distributions can be defined. For each individual landmark distribution l and observation distribution o the distances computed where the following: A Wesserstein(l_G, o_G), a Kullback-Leibler(l_G, o_G), a SquaredHellinger(l_E, o_E), a Kullback-Leibler(l_E, o_E) and Kullback-Leibler(l_C, o_C).

With that in mind the distance between every distribution can be transposed of a vector where each element represents a specific distance between the two distribution. That way, deciding if a cluster is part of a landmark that has been encountered before is now a problem of finding the optimal decision boundary given the distances at hand. For the purposes of this thesis, the decision boundary of an observation being a landmark or not was chosen by empiric evaluation of the landmarks. It is of course possible to learn the optimal decision boundary but due to time restrictions a simpler decision making approach was chosen instead.

4.5. Complexity

The complexity can be decomposed into three parts. The cloud downsampling, the clustering and the decision making process.

$$O(\text{total}) = O(\text{filter}) + O(\text{cluster}) + O(\text{decision})$$

Downsampling: The complexity of the cloud downsampling pipeline can be decomposed to the one of its components. This means that the decomposed complexity is defined as follows:

$$O(\text{filter}) = O(\text{Downsampling} + \text{Stat Removal} + \text{RANSAC} + \text{FPFH} + \text{Color est})$$

Voxel downsampling searches for neighbors within a distance defined by the user and keeps an average value that equally represents the cloud. Since the operation involves searching for neighbors of a point, and since search operations take $O(\log n)$ time where N is the number of points within the cloud, the complexity of voxelGrid downsampling is $O(k \log n)$ where k is the number of neighbors and n the number of points in the cloud. Statistical outlier removal searches for k nearest neighbors and removes those whose deviation is passed a certain threshold. Given that search operations take $O(\log n)$, for k neighbors, the complexity is $O(k \log n)$. The same assumption regarding the averaging computations is done here. A high amount of research has been done regarding the optimal complexity of RANSAC [51]. RANSAC has a complexity of $O(k + m_s * N)$ where k is the maximum amount of iterations defined by the user, m_s the average number of models per sample N the number of data points. FPFH operations have a complexity of $O(nk)$ as given in [22]. Finally, for the operation of color estimation, the k nearest neighbors are chosen and some constant operation is performed on them. The complexity here is similar to Statistical outlier removal since operations after the search are assumed to take take $O(1)$ time. The complexity for color estimation then becomes $O(k \log n)$ where k is the number of neighbors, n the number of points.

The downsampling pipeline has a total complexity of:

$$O(\text{filter}) = O(k_0 \log n_{\text{init}} + k_1 \log n_1 + k_2 + m_s * n_2 + n_3 k_3 + k_4 \log n_3) \quad (11)$$

The different k indexes represent the number of neighbors defined for every operation. The n represents the number of points used as input. Using the notation of equation 11, n_{init} defines the whole cloud, n_1 the cloud after operation 1, n_2 the cloud after operations 2 and so on.

Clustering: The complexity of the SMC sampler is defined in [33] as $O(TLKSN)$ where T defines the time frames, L the number of particles, K the number of clusters, S the number of samples, and N the size of the dataset. Given that the sampler is only used in single timesteps, the computational complexity is reduced to $O(LKSN)$. This is a low complexity and directly affects the performance since the sampler averages 10msec of execution time.

$$O(\text{cluster}) = O(LKSN)$$

Decision making: The decision making takes $O(\kappa * l^2)$ computational time where κ defines the number of clusters output by the sampler and l the number of landmarks currently stored in the database. This number can be further reduced by taking for example only landmarks that are nearby the cluster, but optimizing the decision making performance is outside the scope of this project.

Finally, with some notation abuse, the final complexity of the method can then be defined as:

$$\begin{aligned} & O(\text{filter}) + O(\text{cluster}) + O(\text{decision}) = \\ & O(k_0 \log n_0 + k_1 \log n_1 + O(k_2(t_M) + m_s * n_2) + n_3 k_3 + k_4 \log n_3) + O(LKS_n_3) + O(\kappa * l^2) = \quad (12) \\ & O(k_0 \log n_0 + k_1 \log n_1 + k_2(t_M) + m_s * n_2 + n_3 k_3 + k_4 \log n_3 + LKS_n_3 + \kappa * l^2) \end{aligned}$$

The complexity as defined in equation 12 depends on the initial reduction of the voxel downsampling. As the voxel leaf size parameter decreases and the downsampling outputs a larger cloud, the precision as well as the computing time of the method increases. Since in this thesis the research was directed towards online SLAM methods, the leaf size was modified so that the cloud the time requirements for online landmark tracking were met.

4.6. Landmark size

The basic block of this algorithm is a cluster containing an environment signature. In order to be able to compute how scalable the method is, the size of a single landmark will be computed. Each landmark is represented by a single row in a database[53]. According to the database manual so the maximum number of memory a single landmark might require is 260 bytes. Calculations in the results section are done using 260 bytes as a unit cost of the method.

5. RESULTS

5.1. Simple datasets

In this section the algorithm will be tested against a simple dataset. That will make easier the conceptual extension to more complex clouds that will be used when mapping the environment. In order to test the sampling as well as the decision layer of the algorithm, a simple dataset provided by the pcl[12] library was used. More specifically, a cloud consisting of two milk cartridges with different colors and poses was used. The initial cloud is shown in Fig.12.

The cloud was first given as input to the downsampling and feature extraction pipeline. The reduced cloud(top left Fig.12) was then passed as input to the sampler and the clustering results are shown in Fig.12. The downsampling results in a significantly smaller cloud and this cloud along with feature-information needed to perform the clustering are given as input to the sampler. The sampler outputs a mixture of distributions that fits the input data. The clustering output is shown in Fig.12 with the top right being the Gaussian distributions inferred, bottom left the exponential and bottom right the categorical representing the color information of the cloud. The height of the objects leads to distribution with high variance in the z axis. The sampler outputs 3 clusters for the data and it can be seen that the change in angular information of the box leads the sampler to assign two distributions in the left milk box cloud. The color information is captured correctly in the structures and that was expected since the data had distinct colour signatures.

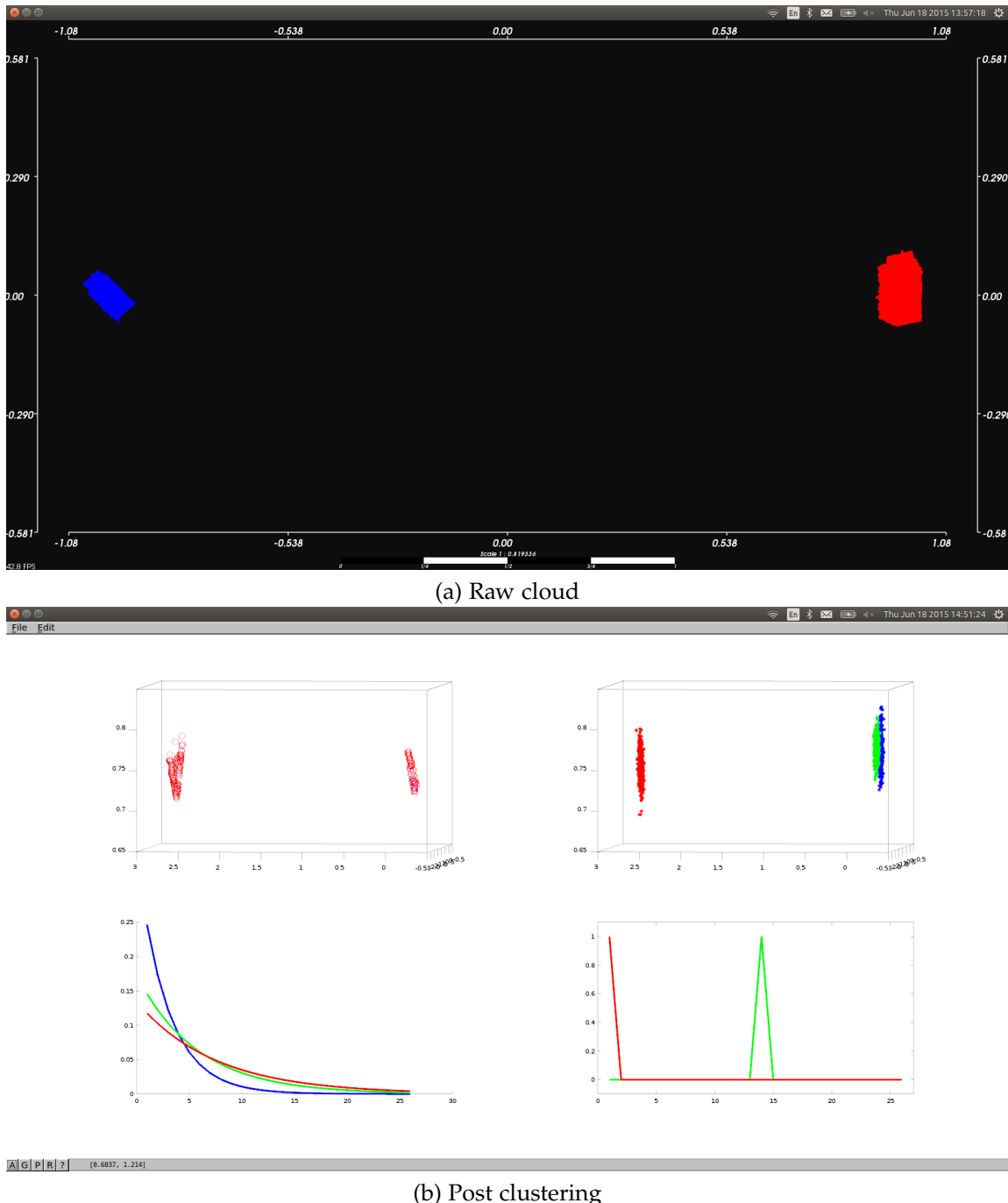


Figure 12: Initial data along with the distributions inferred

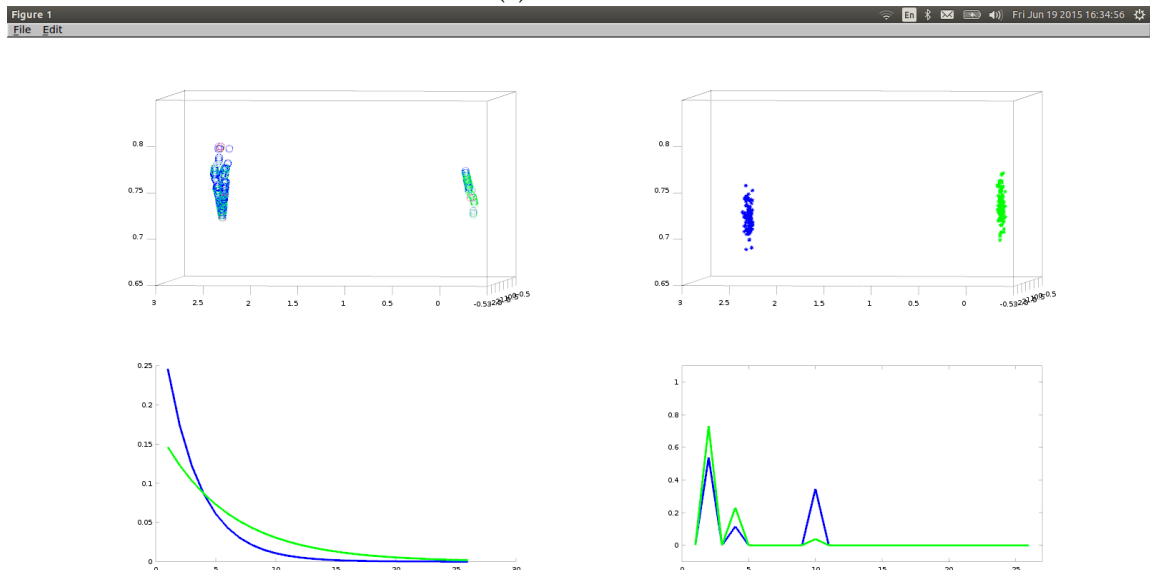
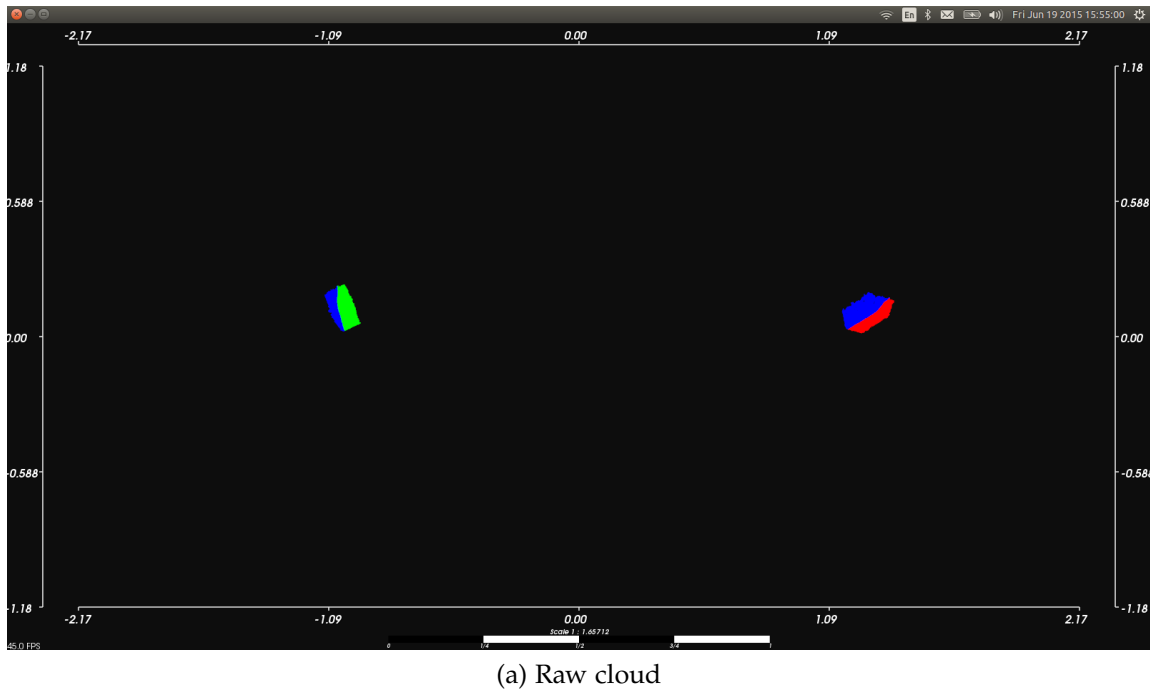
UUID 1					
LandUUID	GausKL	GausWes	ExpHel	ExpHel	CatKL
1	0	1.18111e-07	0	0.164045	0
2	0.0115821	53.5171	1.20726	0.319589	0
3	13.5579	22449.9	1.56956	0.376699	13.8155
UUID 2					
1	0.0115821	20.1454	1.7215	0.319589	0
2	5.42101e-20	4.88951e-08	0	0.411668	0
3	12.8379	21458.6	0.474719	0.449769	13.8155
UUID 3					
1	13.5579	31191.5	2.55205	0.376699	13.8155
2	12.8379	65013.8	0.53855	0.449769	13.8155
3	0	2.43346e-07	0	0.481313	0

After the structure is clustered, distances between the elements can be calculated. The table shows the distances between every cluster shown in Fig.12. It can be seen that the first two landmarks have small distances in their Gaussian counterparts since they represent nearby areas and objects in the cloud that are very far apart. The angular distances between them are also not very large. The distinct colors of the milk boxes make the color signatures of the clusters distinct. The calculated distances are then given to the decision layer to calculate if the clusters currently calculated are part of landmarks previously encountered. An example with more complex color signatures is shown in Fig.13. The clouds are now given a mixture of colors and this is passed to the color signature inferred on every cluster in Fig.13. In this case the sampler outputs 2 clusters and the color signatures capture the more complex color signatures as well as the expected overlap correctly.

5.2. Expressiveness and decision layer

To test the expressiveness of the pipeline, experiments were performed to test how the decision layer differentiates over different objects in the cloud. The decision boundary of the pipeline can be decomposed into three basic parts; a positional, a color and an angular boundary. Fig.14 shows the behavior of the decision layer with respect to the Gaussian(positional) and Categorical(color) parts.

In the first picture of Fig.14 the yellow folder along with some of its environment to the left are being assigned to landmark with id 7386. The folder is then removed and a blue trashcan is put in its place. The folder and the trashcan are similar in size and due to that their Gaussian counterparts will not have large distances. Their main difference lies in the color signature they carry. Since the distance in their color is substantial, a new landmark with id 7412 is created to capture the change in the signature of the environment at that place of the map. The different landmark assigned to the cluster can be seen the second picture in Fig.14. The positional decision boundary is displayed in the third and fourth picture of Fig.14. In the initial position the yellow folder is assigned to the green landmark of the cloud. As the object is moved a different position in the cloud, it is being assigned to a different cluster. The reason the cluster is assigned to multiple landmarks is due to the fact that the folder is decomposed to several clusters and each one of them



(b) Post clustering

Figure 13: More complicated color distributions

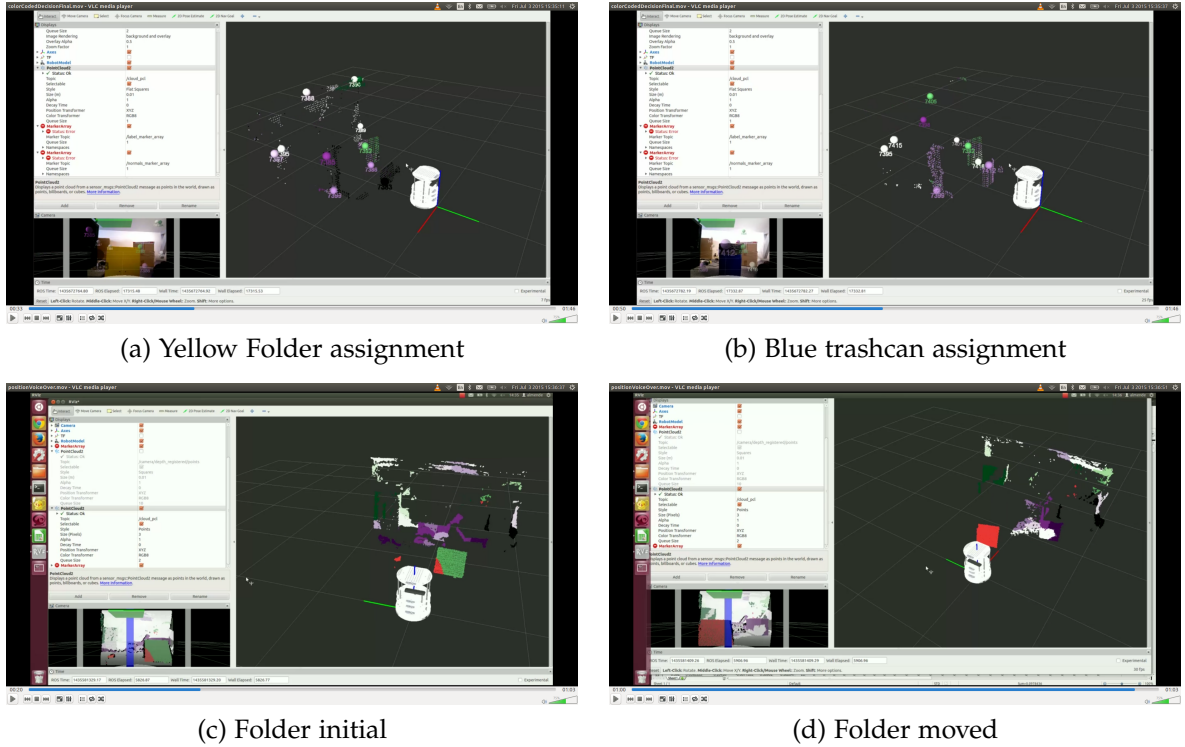


Figure 14: The colour and position boundary is displayed in these pictures

is being assigned to a different part of the cloud with respect to their position. This can be seen in the fourth picture of Fig.14 where the bottom left of the folder is being assigned to the red cluster.

The exponential part of the distribution is responsible for the angle signature elements within a cluster have. Practically, having a large amount of different angle distributions in a single cluster leads to objects that have texture and their surface is not smooth. Having a very strict limit in the angle distribution can lead to very small clusters and subsequently to a high amount of landmarks within the data. Using the data from the kinect camera, angle distributions are highly prone to high amounts of noise that is found in parts of the cloud that are near the end of Kinect sensor's range. Practical evaluation has shown that using an angle limit that is close to the average distance between angle signatures produces stable results and reasonably sized landmarks in the cloud.

5.3. EKF-SLAM experiments

Finally, the pipeline was used in real life scenarios as a sensor model in a Landmark based EKF SLAM algorithm and was tested in its speed and memory requirements. In Fig.15 an end result of a slam session using the pipeline as a sensor model is shown. The yellow spheres represent the landmarks extracted during the slam session with every sphere representing the environment signature at the specific part of the map; noisy cloud readings were taken from a kinect sensor

mounted on the robot.

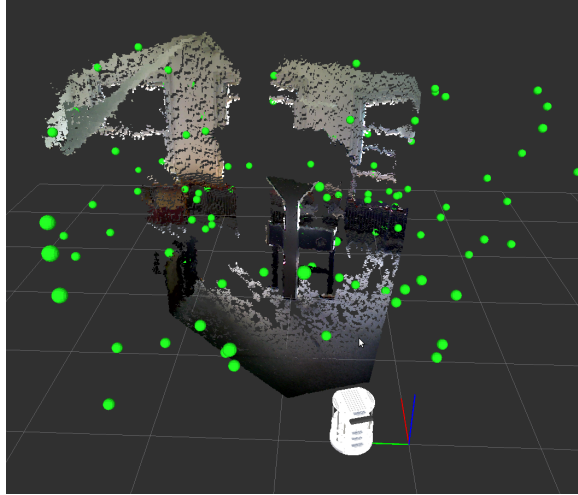


Figure 15: SLAM session using the pipeline.

The compression that the method introduces is not directly observable. As the environment is being reduced from a cloud to a landmarks, the memory needs change from using pointclouds to using the landmarks extracted in those clouds. Since every landmark represents a signature of the environment at this particular point, the compression is done by reducing a high amount of points to that specific signature. The number of parameters needed to define the three distributions in the signature is all the information this method requires and hence the memory gains are substantial. The expressiveness of the distributions greatly affects the objects as well as object shapes that could be represented. Finally it is always possible to extend the method presented by adding new features and new priors to those features.

5.3.1 Speed

As was shown in the Complexity session, the speed is mainly dependent to the initial downsampling of the pipeline. If strong downsampling is performed on the cloud, the information loss will lead to a cloud that does not represent the structure effectively, and, therefore, sub optimal results. Conversely if the downsampling is very loose, the speed of the method will decrease making the pipeline unable to handle online data streams. The speed of the method was tested on a mid level as well as on a high level machine to display the differences in time needed to perform the operations. The benchmark results of a machine running on a pentium i5-3210M and on a pentium i7 are shown in table 5.3.1, and it is clear that speed depends on the initial downsampling process. Furthermore, as will also be shown in the restrictions section, speed also depends on the hyperparameters of the sampler. Having a large alpha value results in a large amount of clusters which also affects directly the speed of the sampler.

Pentium i5-3210M				
Leaf Size	Downs Time	Cloud size	Sampling	Matching
1m	0.908768	9	0.0290296	0.00218081
50cm	0.914169	32	0.0112929	0.00243211
30cm	1.07862	79	0.0138666	0.00126673
10cm	1.1764	654	0.0712596	0.00154977
5cm	1.75907	2391	0.215594	0.00181846
1cm	14.3283	25556	5.06356	0.854803
Pentium i7-3610QM				
Leaf Size	Downs Time	Cloud size	Sampling	Matching
1m	0.675993	7	-	-
50cm	0.779975	30	-	-
30cm	0.676315	66	-	-
10cm	0.746999	488	-	-
5cm	0.878036	1827	0.132831	0.00281951
1cm	1.11554	18487	2.69855	0.0021291

The leaf size directly affects the time the cloud takes to be processed in the pipeline as well as the time the sampling takes afterwards. As shown in the table, a leaf size between 1-5cm provides a good balance between speed and precision. Matching benchmarks the time it takes for the method to match all the landmarks to landmarks in the database, or create new ones. It must be noted that adding new landmarks can be a time consuming operation compared to just matching to existing ones. In fact matching everything to existing takes a very small amount of time and can be therefore disregarded.

5.3.2 Memory requirements

The memory requirements are shown in Fig.16 as a function of strength parameter alpha. The compression that the method introduces is significant since even for a very high value of alpha, since the memory needs of the landmarks are smaller than 30KB of memory total. Mapping the same environment using the RTAB mapping method, results in maps that average 84MB of memory. It can be seen that there is a significant compression ratio of 1/2800.

The memory requirements of the method is a function that is directly affected to the α strength parameter of the sampler. As the α parameter increases, the sampler will output more clusters on every iteration. The higher amount the of cluster will result a higher amount of landmarks and, consequently, in larger memory requirements in the method.

As can be seen, the number of landmarks follows the logarithmic trend of the distribution in relation to α . Increasing the alpha value more will not make the algorithm follow the logarithmic trend indefinitely. That is due to the fact that as the alpha increases, the constant decision layer has an upper bound to the number of landmarks it can have. This means that the algorithm will keep adding landmarks until the environment saturates and no new landmarks can be added. It must also be noted that as the alpha parameter is set to higher numbers, the sampler outputs more clusters making it more accurate of the environment descriptor it outputs, but also takes more

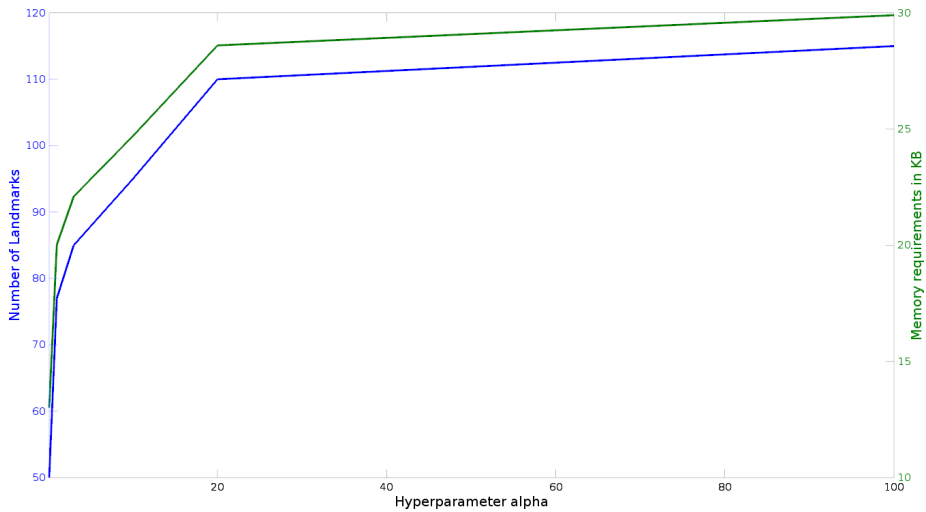


Figure 16: Memory Requirements as a function of strength parameter α .

time, making it non feasible to use this in real time mapping scenarios. Values of alpha between 0 and 10 provide a robust but also fast enough sampler that can be used in online mapping scenarios.

5.4. Discussion

Some important properties of the method with respect to its architecture and behaviour will be discussed in the discussion section.

5.4.1 Unsupervised learning

It is important to note the implications of having a pipeline that is based on a Dependent Dirichlet Process. This means that the pipeline is build on top of an unsupervised learning algorithm. As an extension, the elements of the cloud will be clustered as the algorithm sees (statistically) fit. This means that there will be clusters in the cloud that will be small in size and will contain just parts of objects and, on the other hand, clusters are large contain more than object. One such example is shown in Fig.17 where multiple milk cartridges are either clustered as single entities or part of larger clusters. This approach of representing the environment closely related to how infants create abstractions using simple what-where features[55] that are still informative enough to use in a mapping setting

5.4.2 Clustering layer

An important limit of the pipeline exists with respect to the Dirichlet hyper-parameter α . During the clustering, choosing a correct value for the hyper-parameter α is important. Having the sampler run with a very low α can lead to the whole cloud being assigned a single cluster. Having every

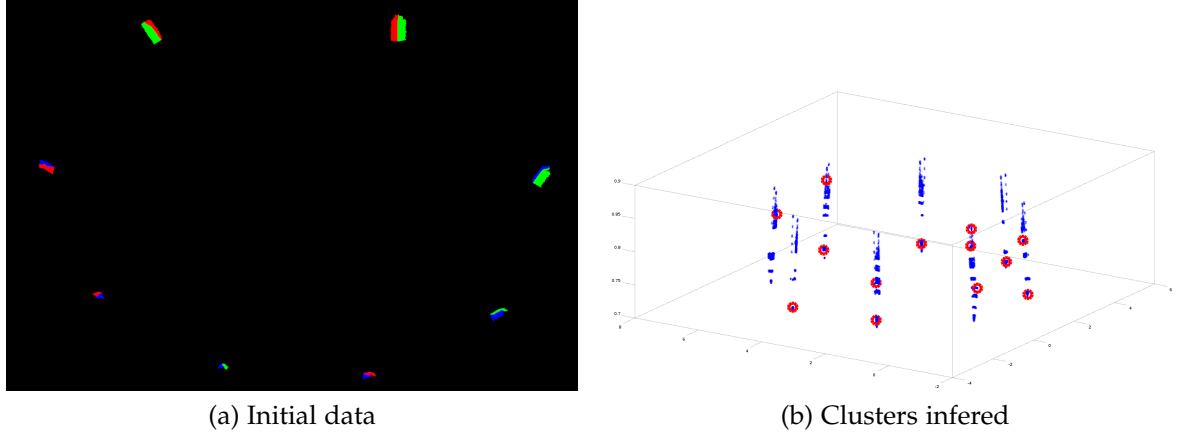


Figure 17: Fail use cases.

point in the cloud being part of the same cluster leads to a significant amount of information loss as no environment specific information are incorporated to the cloud. Fig.[18] shows the behaviour of the sampler for α values lower than 1. The clusters are color coded in the downsampled cloud, and it can be seen that only one cluster is output by the sampler. On the other hand, having a very large α can lead to a very large amount of clusters being output by the sampler every time. That in combination with the strict decision layer can lead to a non converging pipeline since every time a new landmark that does not fit the landmark database is output. This leads to many small clusters with each containing a small number of points. Furthermore, having a high value in the hyperparameter leads to a slower sampling procedure since the complexity of the sampler is $O(TKLSN)$ where K is the number of clusters. Fig.[11] displays the behavior of the sampler for very large values α . The landmarks extracted from a single cloud are shown as spheres; it can be seen that the cloud is not visible and the majority of the points is considered a landmark of its own.

5.4.3 Decision layer

The restrictions introduced by the decision layer are relatively simple due to the simplistic approach of the decision making. Taking very small distances in the distance threshold operation can lead to pipeline that continuously adds new landmarks to the database. An example is shown in Fig. 5.4.3 where limiting the landmark matching operation to very small exponential distances, leads to a cloud where objects are decomposed to many entities that also differ on every iteration. Spheres represent landmarks and it can be seen that the chair is being assigned to many landmarks using the pipeline with this setup. That means that very strict limits lead to a non converging pipeline with respect to the landmarks it outputs. It must be noted that the object decomposition is even more intense when camera movement is involved due to the different angles. Furthermore, since the number of landmarks is also a function of noise, areas of the cloud that are near the maximum range of the sensor can lead to different landmarks added frequently. These issues can be tackled by having a less strict limit in the operation that defines what is considered a landmark

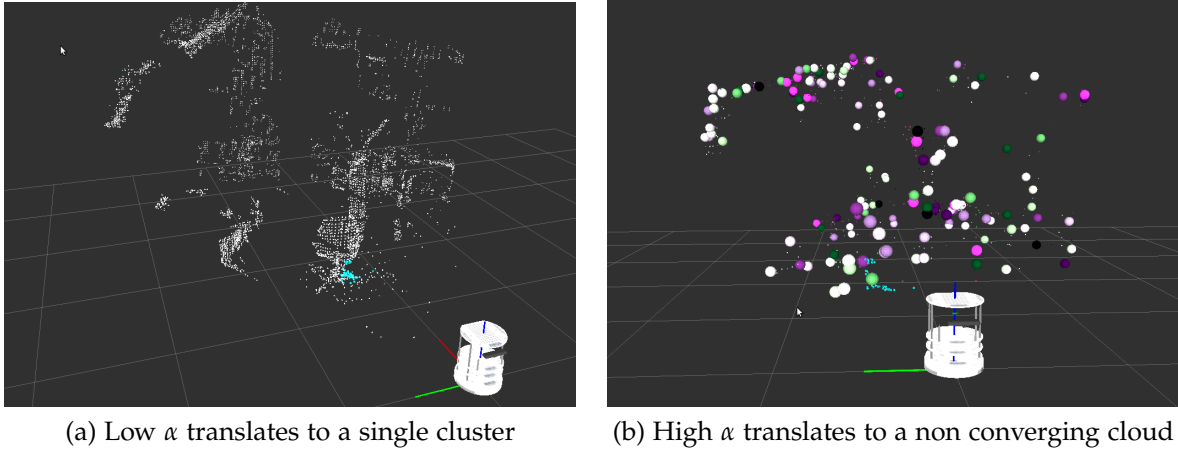


Figure 18: Fail use cases.

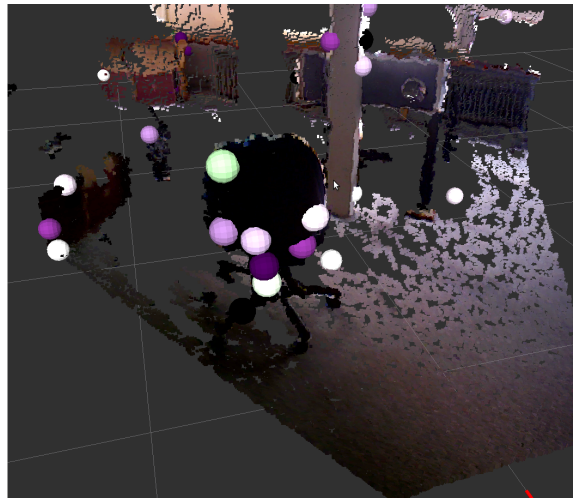
the sampler has encountered before or not.

6. CONCLUSION AND FUTURE WORK

In this paper a novel method for cloud representation using non-parametric Bayesian tools was introduced. Its compression strength and speed were presented as well as how it could help tackle the compression problem of lifelong mapping. The discussion section showed ways that the pipeline can output sub-optimal results and also its clustering behaviour due to its unsupervised nature. There is a number of directions in which the method could be improved. Choosing more complex environment signatures could increase the expressional strength of the sampler making it easier to represent with higher precision more complex structures. Furthermore, since the sampler clusters parts of environment, it would be interesting to see how a hierarchical approach would change the result of the clustering. Hierarchical dependent Dirichlet processes would be interesting extensions since such tools would both have the ability to capture structures in a hierachal way not just as chunks of the environment as well as be able to handle the dynamic component that lifelong mapping problems introduce. Furthermore, having a more complex decision layer would also increase the robustness of the method making it able to handle more complex environment structures. Finally, all those additions could help tackle lifelong mapping problem as a whole in a fully Bayesian manner.

REFERENCES

- [1] Thrun, S. (2002). Probabilistic robotics. Communications of the ACM, 45(3), 52-57.
- [2] Bailey, T., Nieto, J., Guivant, J., Stevens, M., & Nebot, E. (2006, October). Consistency of the EKF-SLAM algorithm. In Intelligent Robots and Systems, 2006 IEEE/RSJ International Conference on (pp. 3562-3568). IEEE.



(a) Very strict decision limits lead to multiple entities on single objects

- [3] Thrun, S., & Montemerlo, M. (2006). The graph SLAM algorithm with applications to large-scale mapping of urban structures. *The International Journal of Robotics Research*, 25(5-6), 403-429.
- [4] Figueiredo, A.J. and Wolf, P. S.A. (2009). Assortative pairing and life history strategy - a cross-cultural study. *Human Nature*, 20:317–330.
- [5] Thrun, S., & Mitchell, T. M. (1995). Lifelong robot learning. *The Biology and Technology of Intelligent Autonomous Agents*, 165-196.
- [6] Konolige, K., & Bowman, J. (2009, October). Towards lifelong visual maps. In *Intelligent Robots and Systems, 2009. IROS 2009. IEEE/RSJ International Conference on* (pp. 1156-1163). IEEE.
- [7] Walcott, A. (2011). Long-term robot mapping in dynamic environments (Doctoral dissertation, Massachusetts Institute of Technology).
- [8] Hjort, N. L., Holmes, C., MÃijller, P., & Walker, S. G. (Eds.). (2010). *Bayesian nonparametrics* (Vol. 28). Cambridge University Press.
- [9] MacEachern, S. N. (2000) Dependent dirichlet processes. Unpublished manuscript, Department of Statistics, The Ohio State University.
- [10] Barber, D. (2012) Bayesian reasoning and machine learning.
- [11] Neiswanger, W., Wood, F., & Xing, E. The dependent dirichlet process mixture of objects for detection-free tracking and object modeling. In *Proceedings of the Seventeenth International Conference on Artificial Intelligence and Statistics* (pp. 660-668) (2014, August)

- [12] Rusu, R. B., & Cousins, S. (2011, May). 3d is here: Point cloud library (pcl). In Robotics and Automation (ICRA), 2011 IEEE International Conference on (pp. 1-4). IEEE.
- [13] LabbAI, M., & Michaud, F. (2011, September). Memory management for real-time appearance-based loop closure detection. In Intelligent Robots and Systems (IROS), 2011 IEEE/RSJ International Conference on (pp. 1271-1276). IEEE.
- [14] Salas-Moreno, R. F., Newcombe, R. A., Strasdat, H., Kelly, P. H., & Davison, A. J. (2013, June). Slam++: Simultaneous localisation and mapping at the level of objects. In Computer Vision and Pattern Recognition (CVPR), 2013 IEEE Conference on (pp. 1352-1359). IEEE.
- [15] Selvatici, A. H., & Costa, A. H. (2008). Object-based visual slam: How object identity informs geometry.
- [16] Castle, R. O., Gawley, D. J., Klein, G., & Murray, D. W. (2007, April). Towards simultaneous recognition, localization and mapping for hand-held and wearable cameras. In Robotics and Automation, 2007 IEEE International Conference on (pp. 4102-4107). IEEE.
- [17] Choudhary, S., Trevor, A. J., Christensen, H. I., & Dellaert, F. (2014, September). SLAM with object discovery, modeling and mapping. In Intelligent Robots and Systems (IROS 2014), 2014 IEEE/RSJ International Conference on (pp. 1018-1025). IEEE.
- [18] Jensfelt, P., Ekvall, S., Kragic, D., & Aarno, D. (2006, September). Augmenting slam with object detection in a service robot framework. In Robot and Human Interactive Communication, 2006. ROMAN 2006. The 15th IEEE International Symposium on (pp. 741-746). IEEE.
- [19] Davison, A. J., Reid, I. D., Molton, N. D., & Stasse, O. (2007). MonoSLAM: Real-time single camera SLAM. Pattern Analysis and Machine Intelligence, IEEE Transactions on, 29(6), 1052-1067.
- [20] Koo, S., Lee, D., & Kwon, D. S. (2014, September). Unsupervised object individuation from RGB-D image sequences. In Intelligent Robots and Systems (IROS 2014), 2014 IEEE/RSJ International Conference on (pp. 4450-4457). IEEE.
- [21] Cichocki, A., & Amari, S. I. Families of alpha-beta-and gamma-divergences: Flexible and robust measures of similarities. Entropy, 12(6), 1532-1568.
- [22] Fast point feature histogram.Rusu, R. B., Blodow, N., & Beetz, M. (2009, May). Fast point feature histograms (FPFH) for 3D registration. In Robotics and Automation, 2009. ICRA'09. IEEE International Conference on (pp. 3212-3217). IEEE.
- [23] Rabbani, T., van den Heuvel, F., & Vosselmann, G. (2006). Segmentation of pointclouds using smoothness constraint. International Archives of Photogrammetry, Remote Sensing and Spatial Information Sciences, 36(5), 248-253.
- [24] Caron, F., Davy, M., & Doucet, A. (2012) Generalized Polya urn for time-varying Dirichlet process mixtures. arXiv preprint arXiv:1206.5254.
- [25] Zhang, Z. (2012) Microsoft kinect sensor and its effect. MultiMedia, IEEE, 19(2), 4-10.

- [26] Wainwright, M. J., & Jordan, M. I. (2008). Graphical models, exponential families, and variational inference. *Foundations and Trends in Machine Learning*, 1(1-2), 1-305. “
- [27] A.Trevor, J.Rogers, and H.Christensen. Omnimapper: A modular multimodal mapping framework. In IEEE International Conference on Robotics and Automation (ICRA), 2014
- [28] Koo, S., Lee, D., & Kwon, D. S. (2013, November). Multiple object tracking using an rgb-d camera by hierarchical spatiotemporal data association. In Intelligent Robots and Systems (IROS), 2013 IEEE/RSJ International Conference on (pp. 1113-1118). IEEE.
- [29] Trevor, A. J., Gedikli, S., Rusu, R. B., & Christensen, H. I. (2013). Efficient organized pointcloud segmentation with connected components. Semantic Perception Mapping and Exploration (SPME).
- [30] Unnikrishnan, R., & Hebert, M. (2003, October). Robust extraction of multiple structures from non-uniformly sampled data. In Intelligent Robots and Systems, 2003.(IROS 2003). Proceedings. 2003 IEEE/RSJ International Conference on (Vol. 2, pp. 1322-1329). IEEE.
- [31] Rabbani, T., van den Heuvel, F., & Vosselmann, G. (2006). Segmentation of pointclouds using smoothness constraint. *International Archives of Photogrammetry, Remote Sensing and Spatial Information Sciences*, 36(5), 248-253.
- [32] Triebel, R., Shin, J., & Siegwart, R. (2010, June). Segmentation and unsupervised part-based discovery of repetitive objects. In *Robotics: Science and Systems* (Vol. 2).
- [33] Neiswanger, W., Wood, F., & Xing, E. (2014, August). The dependent dirichlet process mixture of objects for detection-free tracking and object modeling. In *Proceedings of the Seventeenth International Conference on Artificial Intelligence and Statistics* (pp. 660-668).
- [34] Cree, M. J., Jefferies, M. E., & Baker, J. T. Using 3D Visual Landmarks to Solve the Correspondence Problem in Simultaneous Localisation and Mapping.
- [35] Lowe, D. G. (2004). Distinctive image features from scale-invariant keypoints. *International journal of computer vision*, 60(2), 91-110.
- [36] Lamon, P., Tapus, A., Glauser, E., Tomatis, N., & Siegwart, R. (2003, October). Environmental modeling with fingerprint sequences for topological global localization. In Intelligent Robots and Systems, 2003.(IROS 2003). Proceedings. 2003 IEEE/RSJ International Conference on (Vol. 4, pp. 3781-3786). IEEE.
- [37] Sehgal, A., Cernea, D., & Makaveeva, M. (2010). Real-time scale invariant 3D range pointcloud registration. In *Image Analysis and Recognition* (pp. 220-229). Springer Berlin Heidelberg.
- [38] Neal, R. M. (2000). Markov chain sampling methods for Dirichlet process mixture models. *Journal of computational and graphical statistics*, 9(2), 249-265.
- [39] Blei, D. M., & Jordan, M. I. (2006). Variational inference for Dirichlet process mixtures. *Bayesian analysis*, 1(1), 121-143.

- [40] Montemerlo, M., Thrun, S., Koller, D., & Wegbreit, B. (2002). FastSLAM: A factored solution to the simultaneous localization and mapping problem. AAAI/IAAI, 593-598.
- [41] Teh, Y. W., Jordan, M. I., Beal, M. J., & Blei, D. M. (2006). Hierarchical dirichlet processes. *Journal of the american statistical association*, 101(476).
- [42] Doucet, A., De Freitas, N., & Gordon, N. (2001). An introduction to sequential Monte Carlo methods (pp. 3-14). Springer New York.
- [43] Blei, D. M., Ng, A. Y., & Jordan, M. I. (2003). Latent dirichlet allocation. *the Journal of machine Learning research*, 3, 993-1022.
- [44] MacEachern, S. N. (2000). -
- [45] Fox, E. B., Sudderth, E. B., Jordan, M. I., & Willsky, A. S. (2011). A sticky HDP-HMM with application to speaker diarization. *The Annals of Applied Statistics*, 5(2A), 1020-1056.
- [46] Charles E Antoniak,Mixtures of dirichlet processes with applications to bayesian nonparametric problems, *The annals of statistics* (1974), 1152–1174
- [47] F. Caron, M. Davy, and A. Doucet, Generalized Polya urn for time-varying Dirichlet process mixtures, 23rd Conference on Uncertainty in Artificial Intelligence (UAIâŽ2007), Vancouver, Canada, July 2007, 2007
- [48] Fink, D. (1997). A compendium of conjugate priors.
- [49] AlJilker, Y., GÃijnsel, B., & Cemgil, A. T. (2010). Sequential Monte Carlo samplers for Dirichlet process mixtures. In International Conference on Artificial Intelligence and Statistics (pp. 876-883).
- [50] Del Moral, P., Doucet, A., & Jasra, A. (2006). Sequential monte carlo samplers. *Journal of the Royal Statistical Society: Series B (Statistical Methodology)*, 68(3), 411-436.
- [51] Meer, P., Mintz, D., Rosenfeld, A., & Kim, D. Y. (1991). Robust regression methods for computer vision: A review. *International journal of computer vision*, 6(1), 59-70.
- [52] Raiffa, H. (1974). Applied statistical decision theory.
- [53] <https://www.sqlite.org/datatype3.html>
- [54] Johnson, N. L., & Kotz, S. (1977). Urn models and their application: an approach to modern discrete probability theory (Vol. 77). New York: Wiley.
- [55] Xu, F., Carey, S., & Welch, J. (1999). Infants' ability to use object kind information for object individuation. *Cognition*, 70(2), 137-166.